

Discovery of the nearby long, soft GRB 100316D with an associated supernova

R.L.C. Starling^{1*}, K. Wiersema¹, A.J. Levan², T. Sakamoto^{3,4,5}, D. Bersier⁶, P. Goldoni^{7,8}, S.R. Oates⁹, A. Rowlinson¹, S. Campana¹⁰, J. Sollerman^{11,12}, N.R. Tanvir¹, D. Malesani¹², J.P.U. Fynbo¹², S. Covino¹⁰, P. D'Avanzo¹⁰, P.T. O'Brien¹, K.L. Page¹, J.P. Osborne¹, S.D. Vergani^{13,14}, S. Barthelmy¹⁵, D.N. Burrows¹⁶, Z. Cano⁶, P.A. Curran⁹, M. De Pasquale⁹, V. D'Elia^{17,18}, P.A. Evans¹, H. Flores¹⁴, A.S. Fruchter¹⁵, P. Garnavich¹⁹, N. Gehrels⁴, J. Gorosabel²⁰, J. Hjorth¹², S.T. Holland^{4,21,3}, A.J. van der Horst^{22,23}, C.P. Hurkett¹, P. Jakobsson²⁴, A.P. Kamble²⁵, C. Kouveliotou²², N.P.M. Kuin⁹, L. Kaper^{25,26}, P.A. Mazzali^{27,28,29}, P.E. Nugent³⁰, E. Pian^{31,28}, M. Stamatikos^{4,32,33}, C.C. Thöne¹⁰ and S.E. Woosley³⁴

¹Dept. of Physics and Astronomy, University of Leicester, University Road, Leicester LE1 7RH, UK.

²Department of Physics, University of Warwick, Coventry CV4 7AL, UK.

³Center for Research and Exploration in Space Science and Technology (CRESST).

⁴NASA Goddard Space Flight Center, Greenbelt, MD 20771, USA.

⁵Joint Center for Astrophysics, University of Maryland, Baltimore County, 1000 Hilltop Circle, Baltimore, MD 21250, USA.

⁶Astrophysics Research Institute, Liverpool John Moores University, Birkenhead CH41 1LD, UK.

⁷Laboratoire Astroparticule et Cosmologie, 10 rue A. Domon et L. Duquet, F-75205 Paris Cedex 13, France.

⁸DSM/IRFU/Service DAstrophysique, CEA-Saclay, 91191 Gif-sur-Yvette, France.

⁹Mullard Space Science Laboratory, University College London, Holmbury St. Mary, Dorking, Surrey RH5 6NT, UK.

¹⁰INAF-Osservatorio Astronomico di Brera, Via Bianchi 46, I-23807 Merate (LC), Italy.

¹¹The Oskar Klein Centre, Department of Astronomy, Albanova, Stockholm University, SE-106 91 Stockholm, Sweden.

¹²Dark Cosmology Centre, Niels Bohr Institute, Copenhagen University, Juliane Maries Vej 30, 2100 Copenhagen Ø, Denmark.

¹³University Paris 7, APC, UMR7164 CNRS, 10 rue Alice Domon et Léonie Duquet, 75205 Paris Cedex 13, France.

¹⁴GEPI, Observatoire de Paris, CNRS-UMR 8111, 5 place Jules Janssen, 92195 Meudon, France.

¹⁵Space Telescope Science Institute, 3700 San Martin Drive, Baltimore, MD 21218 USA.

¹⁶Department of Astronomy and Astrophysics, Pennsylvania State University, 525 Davey Lab, University Park, PA 16802, USA.

¹⁷INAF-Osservatorio Astronomico di Roma, Via Frascati 33, I-00040 Monteporzio Catone, Italy.

¹⁸ASI-Science Data Centre, Via Galileo Galilei, I-00044 Frascati, Italy.

¹⁹Physics Dept., University of Notre Dame, Notre Dame, IN 46556, USA.

²⁰Instituto de Astrofísica de Andalucía (IAA-CSIC), Glorieta de la Astronomía s/n, E-18.008 Granada, Spain.

²¹Universities Space Research Association, 10211 Wincopin Circle, Suite 500, Columbia, MD 21044-3432, USA.

²²NASA/Marshall Space Flight Center, Huntsville, AL 35812, USA.

²³NASA Postdoctoral Program Fellow.

²⁴Centre for Astrophysics and Cosmology, Science Institute, University of Iceland, Dunhagi 5, IS-107 Reykjavik, Iceland.

²⁵Sterrenkundig Instituut Anton Pannekoek, University of Amsterdam, P.O. number: 94249, 1090 GE Amsterdam, the Netherlands.

²⁶Laser Centre, VU University, De Boelelaan 1081, 1081 HV Amsterdam, the Netherlands.

²⁷Max-Planck-Institut für Astrophysik, Karl-Schwarzschild-Strasse 1, 85741 Garching, Germany.

²⁸Scuola Normale Superiore, Piazza Cavalieri 7, 56127 Pisa, Italy.

²⁹INAF Oss. Astron. Padova, vicolo dell'Osservatorio 5, 35122 Padova, Italy.

³⁰Computational Cosmology Center, Lawrence Berkeley National Laboratory, 1 Cyclotron Road, Berkeley, CA 94720, USA.

³¹Osservatorio Astronomico Di Trieste, Via G.B. Tiepolo, I - 34143 Trieste, Italy.

³²Center for Cosmology and Astro-Particle Physics (CCAPP) Fellow.

³³Department of Physics, The Ohio State University, 191 West Woodruff Avenue, Columbus, OH 43210, USA.

³⁴UCO/Lick Observatory, Department of Astronomy & Astrophysics, University of California, Santa Cruz, CA95064, USA.

ABSTRACT

We report the *Swift* discovery of the nearby long, soft gamma-ray burst GRB 100316D, and the subsequent unveiling of its low redshift host galaxy and associated supernova. We derive the redshift of the event to be $z = 0.0591 \pm 0.0001$ and provide accurate astrometry for the GRB-SN. We study the extremely unusual prompt emission with time-resolved γ -ray to X-ray spectroscopy, and find that the spectrum is best modelled with a thermal component in addition to a synchrotron emission component with a low peak energy. The X-ray light curve has a remarkably shallow decay out to at least 800 s. The host is a bright, blue galaxy with a highly disturbed morphology and we use Gemini South, VLT and HST observations to measure some of the basic host galaxy properties. We compare and contrast the X-ray emission and host galaxy of GRB 100316D to a subsample of GRB-SNe. GRB 100316D is unlike the majority of GRB-SNe in its X-ray evolution, but resembles rather GRB 060218, and we find that these two events have remarkably similar high energy prompt emission properties. Comparison of the host galaxies of GRB-SNe demonstrates, however, that there is a great diversity in the environments in which GRB-SNe can be found. GRB 100316D is an important addition to the currently sparse sample of spectroscopically confirmed GRB-SNe, from which a better understanding of long GRB progenitors and the GRB-SN connection can be gleaned.

Key words: gamma-ray burst: individual: GRB 100316D; supernovae: individual: SN 2010bh

1 INTRODUCTION

The connection between long-duration gamma-ray bursts (GRBs) and Type Ic core-collapse supernovae (SNe) has long been established, beginning with the association of GRB 980425 with SN 1998bw (Galama et al. 1998; Pian et al. 1998). Subsequent associations between nearby GRBs and spectroscopically-confirmed SNe include GRB 030329/SN 2003dh (Hjorth et al. 2003; Stanek et al. 2003), GRB 031203/SN 2003lw (Malesani et al. 2004) and most recently GRB 060218/SN 2006aj (Campana et al. 2006; Pian et al. 2006). These are spectroscopically confirmed examples of nearby GRB-SN associations (out to $z = 0.17$). The characteristic ‘bump’ of a supernova has been noted in the photometric data for a dozen or more GRBs out to $z \sim 1$ (e.g. Zeh, Klose & Hartmann 2005; Ferrero et al. 2006; Della Valle et al. 2006; Woosley & Bloom 2006; Tanvir et al. 2010), while the majority of GRBs lie at higher redshifts where such signatures would be impossible to detect ($z = 2.2$ Jakobsson et al. 2006; Fynbo et al. 2009). The GRBs with SNe are therefore rare, but provide a crucial insight into the GRB-SN connection and the progenitors of long GRBs.

The GRBs with spectroscopically confirmed SNe are generally underluminous and subenergetic in comparison to a typical long GRB, though GRB 030329 is a notable exception to this. The prompt emission of these bursts has a lower energy spectral peak than a typical GRB (Kaneko et al. 2007) and they are suggested to have less relativistic outflows, or be viewed more off-axis. It has been suggested that the observed nearby ($z < 0.1$), underluminous/subenergetic GRBs, including GRB 100316D, may be drawn from a different population to the cosmological GRB sample, motivated by estimates of the local GRB rate several times greater than the rate of cosmological GRBs (e.g. Cobb et al.

2006; Chapman et al. 2007; Liang et al. 2007). Radio observations of GRBs suggest that mildly relativistic ejecta and often high luminosities are the properties that distinguish the supernovae associated with GRBs from the non-relativistic ordinary Type Ib/c supernovae (Kulkarni et al. 1998; Soderberg et al. 2006).

GRB 060218 was a landmark long-duration, low-luminosity, soft spectral peak event, detected by the *Swift* satellite (Gehrels et al. 2004) with unprecedented multiwavelength coverage of the prompt emission. The prompt spectrum was found to comprise both the non-thermal synchrotron emission ascribed to most GRBs and thought to originate in the collision of fast-moving shells within the GRB jet (e.g. Rees & Mészáros 1994), and a thermal component. The presence of this thermal component, together with its evolution, led to the suggestion that we were observing the shock breakout of the supernova for the first time (Campana et al. 2006; Waxman, Mészáros & Campana 2007). However, the non-thermal emission did not differ greatly from that of the X-ray flash class of soft GRBs and an outflow speed close to the speed of light could be inferred (Toma et al. 2007), alternatively suggesting this to be an extension of the typical GRB population and not requiring significantly slower ejecta or any special (off-axis) geometry (Ghisellini, Ghirlanda & Tavecchio 2007). Toma et al. (2007) speculate that the long-duration, low-luminosity events such as this one may point to a different central engine for these events compared with more typical GRBs: a neutron star rather than a black hole (see also Mazzali et al. 2006; Fan et al. 2010).

Also of relevance to this discussion are the supernovae for which no GRB was detected, yet for which mildly relativistic ejecta provide a good explanation for the radio data: SN 2007gr (Paragi et al. 2010) and SN 2009bb (Soderberg et al. 2010). As GRB jets are thought to be highly collimated, it is expected that many will go unde-

tected if the emission is directed away from our line of sight (e.g. Mazzali et al. 2005), and a fraction will also lie below current detector sensitivity limits. Soderberg et al. (2010) estimate the fraction of Type Ib/c SNe with central engines at about one per cent, consistent with the inferred rate of nearby GRBs. In contrast, there are nearby GRBs for which an accompanying supernova could be expected but none has been detected to extremely deep limits. GRBs 060505 and 060614 (Fynbo et al. 2006; Della Valle et al. 2006; Gal-Yam et al. 2006) are the two best examples of this, highlighting the need for a greater understanding of the relationship between GRBs and SNe.

We present the discovery of a new GRB-SN, GRB 100316D (Stamatikos et al. 2010) associated with SN 2010bh (Wiersema et al. 2010; Bufano et al. 2010; Chornock et al. 2010). This is an unusually long-duration, soft-spectrum GRB positioned on a nearby host galaxy. Many of the properties of this GRB appear unlike those of typical GRBs, resembling rather GRB 060218. In this paper we report accurate astrometry for the GRB-SN and the redshift of the underlying host galaxy. We examine the GRB prompt and afterglow emission observed with all 3 instruments on-board *Swift*, and the broad characteristics of the host galaxy as observed with the Gemini South telescope, the Very Large Telescope (VLT) and the Hubble Space Telescope (HST). We compare these properties with the GRB sample as a whole and with a subset of GRB-SNe, to understand the origins of the GRB emission and further our knowledge of the GRB-SN connection.

2 OBSERVATIONS AND ANALYSES

2.1 *Swift*

On 2010 March 16 at 12:44:50 UT (hereafter T_0), the *Swift* Burst Alert Telescope (BAT, Barthelmy et al. 2005) triggered on and slewed immediately to GRB 100316D (Stamatikos et al. 2010). This was an image trigger, since no rapid, substantial rise in the count rate occurred, but a possible low-level peak about 100 s long was noted in Stamatikos et al. (2010). The X-ray Telescope (XRT, Burrows et al. 2005) on-board *Swift* began observing the field at 12:47:08.1 UT, 137.7 s after the BAT trigger, beginning with 10 s of Windowed Timing (WT) mode settling data and followed by 593 s of WT pointing data. After a time gap due to observing constraints, data-taking recommenced at T_0+33 ks with XRT in Photon Counting (PC) mode. The best X-ray position for this source is the astrometrically corrected XRT position of RA, Dec (J2000) = 07h 10m 30.63s, -56d 15' 19.7", with an uncertainty of 3.7" (radius, at 90% confidence Starling et al. 2010). *Swift*'s UltraViolet-Optical Telescope (UVOT, Roming et al. 2005) began observing with the white filter 148 s after the BAT trigger and continued observations in u band, thereafter cycling repeatedly through all its lenticular filters.

The *Swift* data were processed and analysed with the *Swift* tools version 3.5, released as part of HEASOFT 6.8, and the latest calibration data at 2010 March were used.

XRT WT spectra were grouped with a minimum of 20 counts in each bin, allowing the use of χ^2 statistics, while for the PC spectrum 1 count per bin was required

and Cash statistics used. We fit the X-ray spectra over the energy range 0.3–10 keV and the γ -ray spectra over the range 15–50 keV (as this is a soft event very few counts are present above 50 keV) using the spectral fitting package XSPEC (Arnaud 1996). We used the X-ray absorption models PHABS and ZPHABS for which photoionization cross-sections are taken from Verner et al. (1996) and Solar abundances from Wilms, Allen & McCray (2000). The Galactic absorption in the X-ray band is fixed at 7×10^{20} cm⁻² throughout (Kalberla et al. 2005). We tested for any differences in the spectral fitting results from use of different grade selections or different energy ranges (excluding 0.3–0.5 keV and/or including 50–150 keV) and confirm that these have no effect.

Optical/UV photometry was performed with the UVOT tool UVOTSOURCE. At the position of the SN reported by Levan et al. (2010), background subtracted count rates were extracted using a circular source aperture of 2.5". Source-free background was taken from a region situated outside of the host galaxy. The count rate was aperture corrected to 5" in order to be compatible with the UVOT calibration (Poole et al. 2008). With UVOT we detect the host galaxy, but no new point sources. The 3σ upper limit on any optical transient emission was taken to be the background subtracted count rate plus three times the count rate error and was converted into magnitude using the zero points provided in Poole et al. (2008). At this time, galaxy subtraction cannot be performed since there are no UVOT pre- or post-explosion observations. The host galaxy count rate was determined using an elliptical source region, which enclosed the whole galaxy, and a source-free background region. Photometry of the host was performed on a sum of all data from $\sim 1 \times 10^5$ s after the trigger onwards for each filter. Since the ellipse is similar in area to a 5" circular aperture (semi-major and -minor axes of 7.5" and 5.5" respectively), we have taken the standard UVOT co-incidence loss correction to be the best estimate of the co-incidence loss, and the standard UVOT zero points have been used to convert the count rate into magnitudes.

2.2 Gemini, VLT and HST

Our first optical observations of GRB 100316D were obtained with Gemini-South, starting on March 16 23:53 UT. In these images we identified two point sources, consistent with the initial XRT position (Vergani et al. 2010). We acquired spectroscopy of these with the 3-arm echelle spectrograph X-shooter (D'Odorico et al. 2006), mounted on Unit Telescope 2 of the VLT. These sources were later shown to be compact H II regions unrelated to the supernova. In this paper we will make use of the spectra obtained of the brightest of these two regions, referred to as source 'A' in Vergani et al. (2010) (see Figure 1). We obtained two spectra each of 1200 s exposure of source A, using a 5" nod throw along the slit to achieve better sky subtraction. We used slit widths of 1.0, 1.0 and 0.9" for the UVB, VIS and NIR arms, respectively. Data were reduced using version 0.9.4 of the ESO X-shooter pipeline (Goldoni et al. 2006). Calibration data (bias, dark, arc lamp, flatfield and flexure control frames) were taken the same night. Extracted spectra were flux calibrated using spectrophotometric standard star exposures, also taken the same night, resulting in flux cali-

brated spectra spanning the ultraviolet to the near-infrared ($\sim 300 - 2300$ nm) simultaneously.

We obtained further imaging of the localization with Gemini-South on the subsequent three nights, using these we were able to identify a further bright point source superimposed on the host galaxy (Levan et al. 2010). Image subtraction performed between the different images showed a clear brightening in this source, which we subsequently identified as the associated rising supernova (Wiersema et al. 2010, see Figure 1).

We obtained deep imaging of the position of GRB 100316D using the FORS2 instrument on Unit Telescope 1 of the VLT. Seeing conditions during both epochs were good, averaging $0.8''$, but the second epoch observations suffer from fairly bright background caused by high airmass and a bright moon. The GRB-SN is clearly visible in both epochs.

Following the announcement of a SN discovery (Wiersema et al. 2010), we triggered our cycle 17 HST programme. Here we report the first epoch, obtained on March 25, ~ 9 days after the BAT trigger.

The details of the ground-based and HST observations can be found in Table 1. The data were reduced using standard procedures in IRAF.

3 ASTROMETRY AND REDSHIFT

Subtraction of early from late images taken with Gemini-South reveals a variable source inside the X-ray error circle which we conclude is GRB 100316D/SN 2010bh (Figure 1). We find an accurate position for this variable source by astrometrically calibrating the images, using 190 USNO-B stars in the field. We determine the position of the residual in the image subtraction by using a Gaussian centroiding. This gives a position for the supernova of RA, Dec (J2000) = $07^{\text{h}} 10^{\text{m}} 30.558^{\text{s}}$, $-56^{\circ} 15' 20.18''$ ($\pm 0.26''$). The error is dominated by the scatter of the USNO positions around the best fitting polynomial of the astrometric calibration. We refine this using an image taken with HST, to our best position of RA, Dec (J2000) = $07^{\text{h}} 10^{\text{m}} 30.530^{\text{s}}$, $-56^{\circ} 15' 19.78''$ ($\pm 0.05''$).

We detect a large number of nebular emission lines commonly found in star forming regions with good signal to noise in the VLT X-shooter spectrum of source A (see Section 7, Figure 5). From the 12 brightest lines we measure the redshift $z = 0.0591 \pm 0.0001$. Using the cosmology $\Omega_{\text{M}} = 0.27$, $\Omega_{\Lambda} = 0.73$ and $H_0 = 71 \text{ km s}^{-1} \text{ Mpc}^{-1}$, the luminosity distance is 261 Mpc.

4 TEMPORAL CHARACTERISTICS OF THE PROMPT EMISSION

The BAT and XRT early emission light curves are shown in Figure 2. The γ -ray emission was detected at the 10σ level at $T_0 - 475$ s, prior to which there was no detected emission at 5σ or above. The emission peaked at $T_0 - 100$ s, and decayed with an exponential decay constant of 750 s. Emission continued through the slew at $T_0 + 750$ s. BAT re-observed at $T_0 + 5050$ s from which time γ -ray emission was no longer detected.

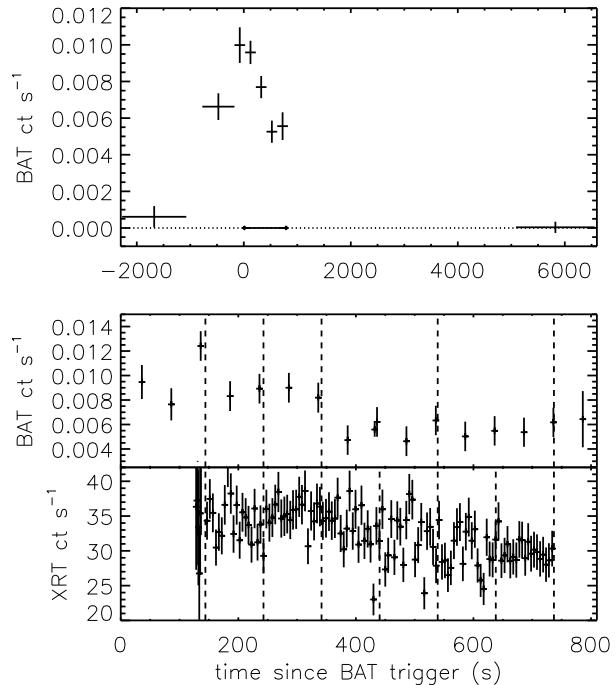


Figure 2. Top panel: 14–195 keV long-term BAT light curve, comprising both event and survey binned data. The zero count rate level is indicated with a dashed line, and the time range covered by the panels below is overlaid as a double-sided arrow. Lower two panels: zoom in on the 14–195 keV BAT event light curve and 0.3–10 keV XRT light curve from T_0 to $T_0 + 810$ s. The dashed lines indicate time slices adopted for spectral fitting.

The prompt emission duration of this GRB is one of the longest ever measured. GRB 100316D was detected with BAT from $\sim T_0 - 500$ s to at least $\sim T_0 + 800$ s, hence the lower limit on the duration of GRB 100316D is ~ 1300 s. The fluence, derived from the 15–150 keV spectrum accumulated between $T_0 - 475.0$ and $T_0 + 795.0$ s since trigger, is $S_{\nu} = (5.10 \pm 0.39) \times 10^{-6} \text{ erg cm}^{-2}$. We note that as γ -ray emission continued after this time but *Swift* was unable to observe, this should be considered a lower limit to the burst fluence. The isotropic equivalent energy that follows from this is $E_{\text{iso}} \geq (3.9 \pm 0.3) \times 10^{49} \text{ erg}$. This is valid for the energy range 15–150 keV, but if we extrapolate down to 1 keV given that this is a soft burst, we find that the fluence and therefore E_{iso} may be higher by 50% leading to $E_{\text{iso}} \geq (5.9 \pm 0.5) \times 10^{49} \text{ erg}$. We note that little flux is observed above 50 keV; the contribution to the isotropic energy from very high energy γ -rays is likely to be small.

The BAT and XRT simultaneous coverage spans 603 s. The XRT count rate light curve decays very slowly with $\alpha = 0.13 \pm 0.03$ throughout this interval.

No variable optical or UV source has been detected during *Swift* observations with the UVOT, hampered by the bright underlying host galaxy (Oates, De Pasquale & Stamatikos 2010). The light curves for each filter are consistent with a constant value, and we confirm that no variable source is detected with image subtraction using the full UVOT dataset to date. Upper limits on the magnitudes of any source at the GRB position are given in Table 2.

Table 1. Log of Gemini-South, VLT and HST observations.

Date start (UT)	Telescope/instrument + filter/arm	T_{exp} (s)	Comments
2010-03-16, 23:53	Gemini-S/GMOS r	5×180	
2010-03-17, 00:58	VLT/X-shooter UVB+VIS+NIR	2×1200	region A
2010-03-17, 23:55	Gemini-S/GMOS r	5×180	
2010-03-18, 23:48	Gemini-S/GMOS r	5×180	
2010-03-20, 00:28	Gemini-S/GMOS griz	3×60	
2010-03-24, 00:07	VLT/FORS2 R _{special}	180	
	VLT/FORS2 I _{Bessel}	180	
	VLT/FORS2 V _{high}	180	
2010-03-25, 04:38	HST/WFC3/UVIS F555W	2×60	
2010-03-29, 01:11	VLT/FORS2 V _{high}	6×150	SN saturated
	VLT/FORS2 R _{special}	17×50	
	VLT/FORS2 I _{Bessel}	9×75	
	VLT/FORS2 V _{high}	17×50	

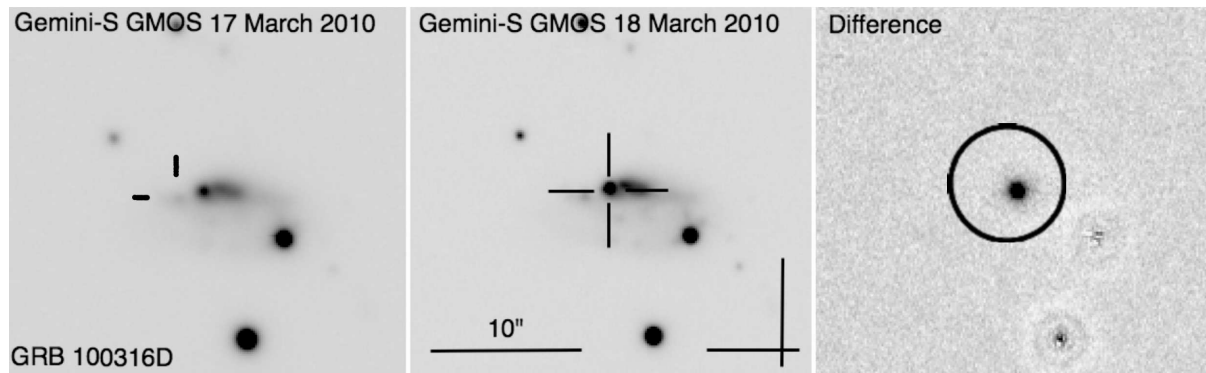

Figure 1. Our Gemini-South discovery images of SN 2010bh, associated with GRB 100316D. The r-band images, obtained one night apart, clearly show the afterglow/SN superimposed on its host light. The GRB/SN position, image scale and North and East directions are indicated in the middle panel. The star forming region ‘A’ is indicated in the left panel. The result of PSF matched image subtraction is shown in the right hand panel, revealing a brightening of the transient. The *Swift* XRT error circle is overlaid on this panel.

Table 2. UVOT 3σ upper limits on the magnitude at the position of the SN, from event and image data. We note that these are background subtracted but not host-subtracted. The time ranges were chosen to overlap with the simultaneous BAT-XRT coverage.

Filter	T_{mid} (s since BAT trigger)	T_{exp} (s)	Magnitude
white	195	93	>21.3
	270	54	>21.0
	597	19	>20.3
v	647	19	>18.4
b	650	22	>19.6
u	324	35	>19.3
	440	194	>20.6
	634	36	>19.4
uvw1	696	19	>18.2
uvm2	671	19	>17.6

5 SPECTRAL CHARACTERISTICS OF THE PROMPT EMISSION

We have carried out time-resolved spectroscopy during the 593 s of BAT-XRT overlap from T_0+144 s to T_0+737 s. For the X-ray data, we take six consecutive time slices, each of ~ 99 s duration. We fit an absorbed power law model, and then include a further blackbody component (Figure 3). In either case the X-ray spectral shape appears stable throughout the WT observations. The intrinsic absorption measured in both sets of fits is consistent at each epoch. We then fit the time-averaged WT spectrum consisting of data from T_0+144 to T_0+737 s since trigger to obtain the best constraints on the intrinsic column which we use in the following BAT-XRT joint fits. The time-averaged WT spectrum and the time-sliced WT spectra are adequately fit with an absorbed power law model, however the inclusion of a blackbody provides a significant improvement in the fits (F-test probabilities of 10^{-10} and 10^{-6} respectively), requiring a larger intrinsic absorption column to accommodate

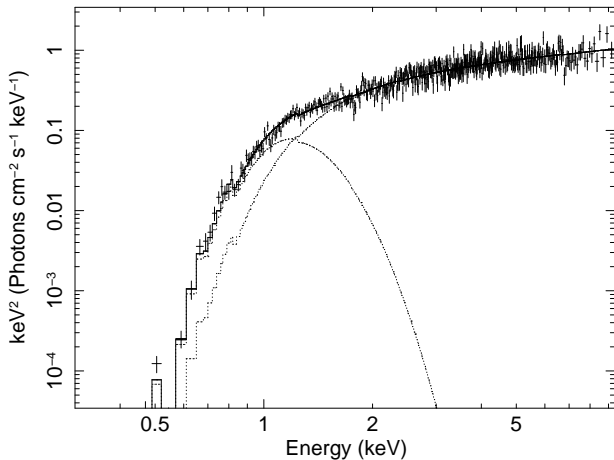


Figure 3. Unfolded XRT WT time-averaged spectrum, EF_E vs. E , with an absorbed power law plus blackbody model, showing the contributions of the two components.

a $kT = 0.14 \pm 0.01$ keV blackbody component while the power law photon index remains approximately the same. The blackbody component contributes $\sim 3\%$ of the total 0.3–10 keV X-ray flux in this model, and has a luminosity of $(3\text{--}4) \times 10^{46}$ erg s^{-1} corresponding to an emitting radius of 8×10^{11} cm. The blackbody luminosity and temperature (Figure 4) are consistent with remaining constant until at least $T_0 + 800$ s.

In order to more rigorously test the significance of the blackbody component, we simulated 10000 spectra based on the absorbed power law model that best fits the time-averaged WT spectrum of GRB 100316D (Table 3). We fitted the simulated spectra with absorbed power law plus blackbody models to recover the chance probability that adding a blackbody component significantly improves the fit, following the methodology described in Hurkett et al. (2008). There were no simulated spectra for which $\Delta\chi^2$ indicated an improvement in the fit comparable to that found in our data, implying that the blackbody component in the time-averaged WT spectrum of GRB 100316D is $> 4\sigma$ significant. This test gives us a high degree of confidence in our identification of a thermal component in the X-ray spectrum at early times.

The joint BAT-XRT fits were performed with two 99 s and two 198 s consecutive time slices. We fit these spectra with an exponentially cut-off power law model¹ with and without a blackbody component. A constant normalisation ratio between the BAT and XRT spectra (to account for calibration uncertainties in the response matrices of the different instruments) is not included in the reported fits since we found this to be 0.9 ± 0.2 , i.e. consistent with unity. The exponentially cut-off power law model provides a good fit with a stable low energy power law slope of $\Gamma \sim 1.4$. The peak energy is at ~ 30 keV in the first time interval and moves to lower energies with time (Figure 4). To estimate the spectral shape during and prior to the BAT trigger we fitted the BAT spectrum from $T_0 - 175$ to $T_0 + 144$ s simultaneously with the time-averaged WT spectrum, given that

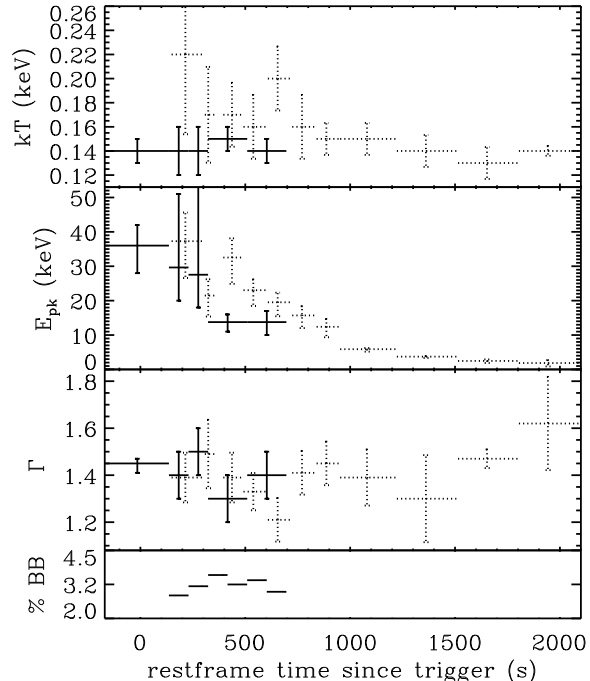


Figure 4. Evolution of power law photon index Γ , peak energy E_{pk} and blackbody temperature kT in the blackbody plus exponentially cut-off power law model fitted to the BAT-XRT spectra for GRB 100316D (solid error bars), compared with the same model fitted to BAT-XRT data of GRB 060218 (taken from Kaneko et al. 2007, dotted error bars) in the source rest-frames. Errors are 90% confidence. The bottom panel shows the percentage contribution of the blackbody component to the total observed 0.3–10 keV X-ray flux, in time-sliced XRT spectral fits to GRB 100316D.

no significant X-ray spectral evolution is observed in the interval 144–737 s. We stress that because the data are not simultaneous this fit provides only an indication of the spectral shape at early times. Spectral fitting results are given in Table 3.

The latest time slice taken for our joint BAT-XRT fits also has full coverage in the u band with UVOT. We have included the u band 3σ upper limit and refit the data with an absorbed and reddened blackbody+power law model. We obtain an acceptable fit, when the underlying spectrum is fixed in shape as listed in Table 3, with an intrinsic extinction of $E(B - V) \sim 0.9$ mag or $A_v \sim 2.6$ mag using the Small Magellanic Cloud extinction law (Pei 1992, fixing the Galactic extinction to $E(B - V) = 0.12$ mag according to Schlegel, Finkbeiner & Davis 1998). This provides a lower limit on the host galaxy extinction along the line-of-sight to the GRB, only under the assumption that any optical transient emission lies on an extrapolation of the high energy spectrum. A measurement of the optical extinction along the line-of-sight to the GRB can be made with spectroscopy of the supernova, for example through the strength of interstellar medium Na I lines (Bufano et al. in preparation).

¹ defined as $A(E) = E^{-\Gamma} e^{-E(2-\Gamma)/E_{pk}}$

Table 3. Spectral fits to the *Swift* BAT and XRT data with an absorbed power law (PL) or cut-off power law (CPL) model, with and without a blackbody (BB) component. Errors are quoted at the 90% confidence level. Galactic absorption is fixed at $7 \times 10^{20} \text{ cm}^{-2}$.

[†] These parameters are tied together for all time intervals.

* XRT data are not available during this time. We perform this fit only to provide an indication of the cut-off power law parameters over this time interval, using the time-averaged WT spectrum given that no significant X-ray spectral evolution is detected in the interval 144–736 s. Therefore this fit was performed separately rather than simultaneously with the 144–736 s interval BAT-XRT time-sliced fits.

	PL or CPL			PL+BB or CPL+BB			
T (s since BAT trigger)	$N_{\text{H,int}}$ (10^{22} cm^{-2})	Γ	E_{pk} (keV)	$N_{\text{H,int}}$ (10^{22} cm^{-2})	kT (keV)	Γ	E_{pk} (keV)
XRT WT time-averaged: 144-737	$\chi^2/\nu = 587.9/480$			$\chi^2/\nu = 538.8/478$			
	0.91 ± 0.05	$1.40_{-0.03}^{+0.04}$	-	1.83 ± 0.06	0.14 ± 0.01	1.53 ± 0.06	-
XRT WT time-sliced: 144-243	$\chi^2/\nu = 830.9/754$			$\chi^2/\nu = 782.1/742$			
	$0.90 \pm 0.05^{\dagger}$	1.35 ± 0.06	-	$1.8 \pm 0.2^{\dagger}$	0.14 ± 0.02	1.5 ± 0.1	-
243-342	"	1.41 ± 0.06	-	"	0.14 ± 0.02	1.6 ± 0.1	-
342-440	"	1.36 ± 0.06	-	"	0.15 ± 0.02	1.5 ± 0.1	-
440-539	"	1.43 ± 0.06	-	"	$0.14_{-0.02}^{+0.03}$	1.6 ± 0.1	-
539-638	"	1.43 ± 0.06	-	"	0.13 ± 0.02	1.5 ± 0.1	-
638-737	"	1.40 ± 0.06	-	"	$0.14_{-0.02}^{+0.03}$	1.6 ± 0.1	-
XRT PC time-averaged: 32906-508263	C-statistic/ $\nu = 13.8/15$			C-statistic/ $\nu = 15.4/15$			
	0.90 fixed	3.5 ± 1.0	-	1.83 fixed	-	$4.6_{-1.3}^{+1.6}$	-
BAT: -175-144	$\chi^2/\nu = 16.0/14$						
	-	2.1 ± 0.4	-				
BAT-XRT: -175-144*	$\chi^2/\nu = 617.4/518$			$\chi^2/\nu = 572.1/516$			
	0.90 fixed	1.33 ± 0.03	33_{-5}^{+7}	1.83 fixed	0.14 ± 0.01	$1.45_{-0.04}^{+0.02}$	34_{-6}^{+8}
BAT-XRT: 144-243	$\chi^2/\nu = 853.4/768$			$\chi^2/\nu = 806.1/760$			
	0.90 fixed	1.25 ± 0.08	25_{-5}^{+9}	1.83 fixed	0.14 ± 0.02	1.4 ± 0.1	28_{-8}^{+23}
243-342	"	1.32 ± 0.08	22_{-5}^{+9}	"	0.14 ± 0.02	1.5 ± 0.1	26_{-8}^{+36}
342-539	"	$1.24_{-0.07}^{+0.06}$	14_{-2}^{+3}	"	0.15 ± 0.01	1.3 ± 0.1	13_{-2}^{+3}
539-737	"	1.28 ± 0.07	14 ± 3	"	0.14 ± 0.01	1.4 ± 0.1	13_{-3}^{+4}

6 THE LATE-TIME BEHAVIOUR

The X-ray emission after 10^4 s decayed more steeply than did the emission during the first 800 s after the BAT trigger. Treating the early and late X-ray emission separately, we fit only the data after 10^4 s with a power law decay. This results in an acceptable fit, with $\alpha = 1.35 \pm 0.30$.

The XRT count rates for this source lie within the spread of the entire XRT GRB light curve sample at all observed times, however its shape is atypical. Four light curve types were identified in the *Swift* XRT catalogue, to which 76% of their sample could be ascribed (Evans et al. 2009). GRB 100316D appears not to fit any of these light curve types, if all the early data are included.

The X-ray spectrum from $T_0 + 3 \times 10^4$ to 5×10^5 s allows only poor constraints on the parameters of an absorbed power law model, but we find it is significantly spectrally softer at this time than in the earlier WT data. Using Cash statistics, and fixing the intrinsic absorption to that found in the combined WT spectrum, we find the power law has a photon index of $\Gamma = 3.5 \pm 1.0$ (Table 3). This is a very high value, or a very soft spectrum, that although not unique among *Swift* bursts (see e.g. Evans et al. 2009) is difficult to accommodate within the standard fireball model generally used to explain GRB afterglow emission (e.g. Sari, Piran & Narayan 1998), but may possibly be explained with inverse Compton scattering (e.g. Waxman et al.

2007). The temporal decay rate, however, is rather typical of GRB afterglows.

We now turn to the optical regime, to estimate the supernova contribution at the epochs of our VLT data. We performed point spread function (PSF) matched image subtraction on the FORS2 images, using the ISIS2 code (Alard 2000). For the second epoch V_{high} data we use the short exposure time images, as the frames with longer exposure time show the supernova to be somewhat saturated. The subtraction shows a residual at the position of the supernova associated with this GRB (Wiersema et al. 2010) in the V and I bands, whereas the subtraction is too noisy in the R band. This residual shows that the supernova is fainter in the second FORS2 epoch than in the first epoch, at least in V and I, suggesting that the supernova peaked in these bands between 8 and 13 days after burst. This is similar to the SN 2006aj (GRB 060218), which peaked at 10.2 ± 0.3 days after burst in V (Ferrero et al. 2006; Mirabal et al. 2006; Modjaz et al. 2006; Sollerman et al. 2006).

7 THE HOST GALAXY

The deep Gemini, VLT and HST observations show a bright, blue galaxy, covering the $3.7''$ radius refined XRT error circle (Figures 1 and 8). The galaxy has a highly disturbed morphology, but is dominated by a central bright region, possibly the galaxy nucleus, and an arc-like shape resembling

a spiral arm. The galaxy hosts a large number of knots, or blobs, likely giant HII regions. Colour differences between these knots can be discerned, caused by differences in age, metallicity, reddening or a combination of these. The supernova itself is located on top of a bright, blue knot, close (in projection) to the possible galaxy nucleus. The UVOT also observed the host galaxy in all filters and approximate magnitudes, uncorrected for extinction and including an unknown level of contamination by the afterglow and/or SN, are reported in Table 4.

It has long been contended that the properties of the host galaxies of GRBs can provide additional clues to the progenitor evolution, through determination of properties such as the age, metallicity and alpha element enrichment of the stellar population. The low redshift GRB-SNe are of particular interest, as they allow one to obtain spatially resolved spectroscopy (e.g. Christensen et al. 2008). The derived properties can then be meaningfully compared to those of ‘normal’ core-collapse supernova hosts (Fruchter et al. 2006; Svensson et al. 2010) or other star forming galaxy populations. For these reasons we analyse the X-shooter spectrum we obtained of a bright HII region within the host, which we call source A (Vergani et al. 2010), spatially distinct from the supernova region (Figures 1 and 8). We choose to use this spectrum rather than the X-shooter spectra of the supernova itself, as in these spectra the contribution of the supernova to the spectrum is large and can not be easily separated from the underlying HII region lines. Source A is located near the supernova (projected distance approximately 2 kpc) and we may expect the properties of this region to give a meaningful insight into the properties of the host as a whole.

We detect a large number of nebular emission lines commonly found in star forming regions; a selection of those used here (which are all unresolved) is shown in Figure 5. We use the Balmer H α and H β line fluxes to measure a value for the Balmer decrement (jointly fitting the stellar Balmer absorption component and the nebular emission line component), assuming case B recombination (e.g. Osterbrock 1989; Izotov, Thuan & Lipovetsky 1994). Assuming an electron temperature of 10^4 K we compute the extinction (we find $E(B-V) = 0.178$ mag for the combination of Galactic reddening of $E(B-V)_{\text{gal}} = 0.07$ mag and intrinsic reddening in source A), and deredden the spectrum accordingly.

We compute the average electron density n_e using the [SII] doublet and the [OII] doublet: both of the doublet flux ratios are consistent with their lower limits, so we assume a value of $n_e = 100 \text{ cm}^{-3}$ (see e.g. Osterbrock 1989). The electron temperature sensitive [OIII] $\lambda 4363$ and [OII] $\lambda \lambda 7320, 7331$ doublet are detected, from which we calculate the electron temperatures for O^{2+} and O^+ directly (e.g. Osterbrock 1989), at 11880 ± 800 K and 10400 ± 1100 K, respectively (errors are 1σ). Ionisation corrections to account for the presence of O^{3+} were found to be negligible, also evidenced by the non-detection of HeII $\lambda 4686$, so we determine the oxygen abundance in region A as $\text{O}/\text{H} = \text{O}^+/\text{H}^+ + \text{O}^{2+}/\text{H}^+$. Using the measured line fluxes, densities and temperatures we arrive at an electron temperature based oxygen abundance of $12 + \log(\text{O}/\text{H}) = 8.23 \pm 0.15$ in region A (0.37 times Solar metallicity, assuming a solar oxygen abundance of $12 + \log(\text{O}/\text{H}) = 8.66$; Asplund et al. 2004). We note that a similar oxygen abundance has

Table 4. UVOT observed magnitudes and 1σ errors for the host galaxy. Photometry is performed as described in Section 2.1. N.B. any afterglow or supernova contribution is uncertain so could not be removed, however no variability is seen in subtraction of late-time images from earlier epochs.

Filter	T_{start} (s since BAT trigger)	T_{stop}	T_{exp} (s)	Magnitude
v	1.1×10^5	6.1×10^5	3229	17.71 ± 0.03
b	1.1×10^5	6.1×10^5	3578	18.29 ± 0.03
u	1.1×10^5	6.1×10^5	4325	18.02 ± 0.03
uvw1	1.1×10^5	6.3×10^5	8851	18.07 ± 0.03
uvm2	1.1×10^5	6.1×10^5	8332	17.99 ± 0.03
uvw2	1.1×10^5	6.1×10^5	16226	18.00 ± 0.02

been derived from spectra at the SN site (see Chornock et al. 2010).

In the spectrum we detect Balmer absorption lines underlying the nebular emission. This is common in GRB host galaxy spectra, and can provide a useful age tracer, providing the spectra have sufficient resolution (e.g. Wiersema et al. in preparation). We fit the H δ absorption component, and find an approximate age for the dominant stellar population of ~ 30 Myr, assuming continuous star formation (Gonzalez Delgado, Leitherer & Heckman 1999). We also note the absence of obvious Wolf-Rayet star emission line features in source A. The detection of the bright H α line allows us to estimate the star formation rate at location A: the H α line luminosity is a tracer of recent star formation frequently used in nearby GRB host galaxies. We use the expression $SFR_{\text{H}\alpha} = 7.9 \times 10^{-42} L_{\text{H}\alpha}$ (Kennicutt 1998). Using the de-reddened flux from the X-shooter spectrum we find $SFR_{\text{H}\alpha} = 0.17 \text{ M}_{\odot} \text{ yr}^{-1}$. Note that no aperture correction is performed, so this value is formally a lower limit.

A more detailed analysis of the host galaxy will appear in Flores et al. (in preparation).

8 DISCUSSION

GRB 100316D is an atypical gamma-ray burst both in its temporal and spectral behaviour. The very soft spectral peak and extended and slowly decaying flux emission are highly unusual among the prompt emission of GRBs (e.g. Sakamoto et al. 2008). The estimated total isotropic energy ($E_{\text{iso}} \geq (5.9 \pm 0.5) \times 10^{49}$ erg), when considered with the 90% confidence range of spectral peak values of 10–42 keV we measure in Section 5, places GRB 100316D on the low E_{iso} –low E_{pk} tail of the Amati correlation which relates E_{pk} and E_{iso} for the majority of typical GRBs (Amati 2006). The notable outlier to this relation is GRB 980425 (SN 1998bw) (e.g. Kaneko et al. 2007; Amati et al. 2007). We also compare this GRB with the relation reported by Gehrels et al. (2008) between XRT flux at 11 h (here, $(3.2 \pm 0.8) \times 10^{-13}$ erg $\text{cm}^{-2} \text{ s}^{-1}$) and BAT fluence and find, using the lower limit to the fluence, that it lies along the correlation with values that are typical for the sample of *Swift* GRBs reported in Evans et al. (2009).

GRB 100316D is among the longest duration *Swift* GRBs ($T_{90} \geq 1300$ s), after GRB 090417B ($T_{90} \sim 2130$ s) and GRB 060218 ($T_{90} \sim 2100$ s). GRBs with durations of 400 s or longer, as quantified using the T_{90} parameter, ac-

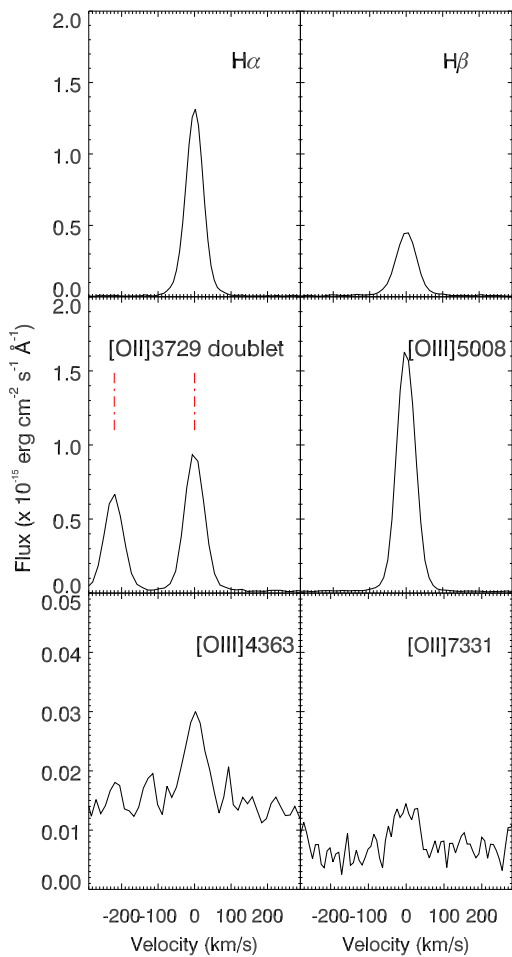


Figure 5. A selection of emission lines which are most important for the oxygen abundance analysis, detected in the X-shooter spectrum of the source ‘A’ HII region in the host galaxy, ~ 2 kpc projection from the GRB/SN location. The top two panels show the Balmer $H\alpha$ and $H\beta$ lines used for the determination of the reddening. The middle panels show the strong lines of the [O II] $\lambda\lambda 3727, 3729$ doublet and [O III] $\lambda 5008$. The zero velocity point for [O II] $\lambda\lambda 3727, 3729$ is (arbitrarily) chosen to be the centre of the redmost component of the doublet. The lower panel shows the temperature sensitive lines of [O III] and [O II] (of the latter only one member of the doublet is shown) from which we derive $T_e(\text{O}^{2+})$ and $T_e(\text{O}^+)$ respectively.

count for only 1.4% of the *Swift* sample observed to date. Owing to their long prompt emission durations, these GRBs are more likely to have exceptional broadband coverage, lending themselves to prompt emission studies. We show the X-ray light curve and hardness ratio of GRB 100316D in relation to the $T_{90} > 400$ s XRT-observed *Swift* events in Figure 6 (omitting GRB 060218 as it can be seen in Figure 7; data are taken from the *Swift* XRT GRB light curve repository², Evans et al. 2007).

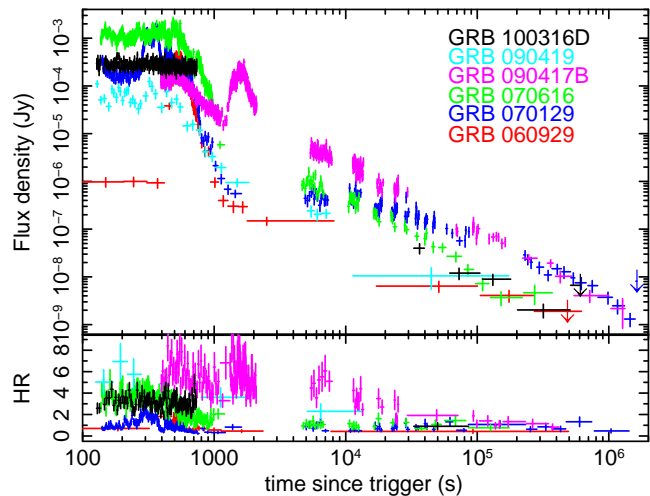


Figure 6. Upper panel: X-ray light curves in flux density at 1.7 keV against time since trigger for a selection of *Swift* XRT-observed very long prompt emission duration (> 400 s) GRBs (excluding 060218). Lower panel: $(1.5\text{--}10\text{ keV})/(0.3\text{--}1.5\text{ keV})$ hardness ratios derived from the XRT count rate light curves.

This category comprises a number of different light curve types, from those which are long due to triggering on a precursor or the presence of a broad flare to the very gradually decaying prompt emission of GRB 100316D. The *Swift* subsample shown here indicates two GRBs, in addition to GRB 060218, whose emission resembles GRB 100316D both in temporal decay and in spectral hardness: GRBs 070616 (Starling et al. 2008) and 090419 (Stratta et al. 2009). We note that GRB 090417B is also spectrally hard at early times, but this may be attributed to strong X-ray flaring (Holland et al. in preparation).

GRB 070616 was particularly well sampled, with γ -ray through optical coverage at early times clearly showing the movement of the spectral peak energy of the Band function (Band et al. 1993) and the occurrence of additional spectral softening (Starling et al. 2008). However, the spectrum was much harder than that of 100316D - observed by both *Swift* BAT and *Suzaku* WAM, and neither the redshift nor the presence of any SN could be established as the source lay close to a bright star.

We now discuss the properties of GRB 100316D in the context of GRB-SNe, paying particular attention to GRB 060218.

8.1 Comparison to GRBs with accompanying supernovae: high energy emission

In Figure 7 we show the X-ray light curves and hardness ratios of a subset of the GRBs with associated SNe (either spectroscopically or photometrically confirmed). On this plot we also include GRB 051109B which was tentatively associated with a very low redshift ($z = 0.08$, Perley et al. 2006) host galaxy and has no reported SN that we are aware of, and the well-studied nearby GRBs 060505 and 060614 for which SN searches to very deep limits registered no detections (Fynbo et al. 2006; Della Valle et al. 2006; Gal-Yam et al. 2006). The prompt emission shows a broader range of observed fluxes than the late-time decays, perhaps

² http://www.swift.ac.uk/xrt_curves/

suggesting they are unrelated or that an extra component is present in the early emission which contributes differently in each GRB. The majority of the GRB-SNe (and GRBs without SNe shown here) light curves decay steeply over the first 1000 s, with GRBs 100316D and 060218 being the only exceptions. The hardness ratios reveal that GRB 100316D and GRB 060218 have a similar spectral hardness evolution, clearly different from those of most other GRB-SNe which remain at a stable and softer spectral shape throughout the prompt and late-time emissions. GRBs 060614 (without a SN) and 090618 (photometrically discovered SN) also transition from hard to soft, but do this earlier, over the first 200 s during their steep decays. We note, however, that X-ray data during the early emission for a number of the GRB-SNe, including the spectroscopically confirmed GRB-SNe 980425, 030329, 031203 and 050525A, are either not available or inadequate for spectral studies.

8.2 Comparison to GRBs with accompanying supernovae: host galaxies

Nearby GRBs show a large variety in their host galaxy properties: the prototype GRB-SN, GRB 980425 and SN 1998bw, occurred in a dwarf spiral, in a small H II region right next to a very large star formation complex; whereas GRB 060218 and SN 2006aj, occurred in a very faint, blue compact dwarf galaxy (Wiersema et al. 2007). This diversity is illustrated in Figure 8.

Assuming that the properties of source A are at least roughly representative of the host galaxy as a whole, we can compare the spectroscopic properties with those of the other nearby GRB-SN hosts. Electron temperature based oxygen abundances have been derived for several of these, see Table 5. The case of GRB 980425 is of particular interest: besides many similarities between SN 1998bw and SN 2010bh there are also several similarities in host galaxy properties. The T_e metallicity measured at the location of the GRB and at the location of a nearby, bright, WR star region (Hammer et al. 2006) are clearly similar to the metallicity measured for the H II region A in the host of GRB 100316D. In addition, the size and brightness (and possibly morphology) of these two hosts are comparable, though an important difference between the host of 980425 and 100316D is evident from Figure 8: the morphology of the host of 100316D is highly disturbed, possibly indicative of a recent merger.

The host of GRB 980425 has been studied using integral field spectroscopy (Christensen et al. 2008), showing that the H II region in which the GRB exploded is similar in mass, SFR, reddening and line equivalent width to other H II regions in this host, with the exception of a bright WR-star rich H II region 800 pc away from the GRB site. In terms of metallicity, the WR region and GRB site have a somewhat lower metallicity than other H II regions in this host (Christensen et al. 2008). If this situation is comparable to the host of GRB 100316D, we may expect that the properties measured above of source A are indeed representative of most of the host galaxy properties.

8.3 Comparison to GRB 060218

In Section 8.1 we found that among the GRB-SNe, there is a clear commonality in the X-ray behaviour of 100316D

and 060218. Comparing the prompt emission spectra in Section 5, we again find parallels in that both bursts seem to require a similar thermal component in addition to the typical GRB synchrotron emission for which the synchrotron peak is observed to move to lower energies with time. The time-evolving prompt spectral parameters are compared in Figure 4. Both events have low isotropic equivalent energies, of order 4×10^{49} erg, and very little flux above 50 keV.

These two events lie in apparently quite different environments: 060218 in a faint, compact dwarf (Wiersema et al. 2007; Modjaz et al. 2006) and 100316D in a luminous, disturbed possibly spiral host galaxy. The metallicities are also different, with the host of 100316D likely being more metal-rich (though the metallicity is below Solar). A prompt optical component, as observed in 060218, could not be detected in 100316D, but conditions for its detection were far less optimal in this case due to the superposition on a brighter host galaxy and the possibility of a higher extinction along the line-of-sight. The higher intrinsic X-ray column density we measure for 100316D compared with similar modelling of 060218 does not necessarily imply a higher optical extinction (Watson et al. 2007; Campana et al. 2010).

In summary, both 100316D and its predecessor 060218 are nearby ($z = 0.059, 0.033$), long-duration ($T_{90} \geq 1300$ s, 2100 s), initially relatively constant in X-ray flux (Figure 6), spectrally soft (very few or no counts above 100 keV; low E_{pk} , Figure 4), subenergetic (both have $E_{iso} \sim 4 \times 10^{49}$ erg) GRBs with an associated SN. These two events show similar prompt emission properties and stand out among the GRB-SNe subsample considered here for their unusual X-ray evolution. However, their host galaxies are rather different in morphology and metallicity, with the host of 100316D more closely resembling the host of 980425.

The thermal X-ray component, with a luminosity, temperature and radius similar to that observed in 060218, dictates that the shock break-out of the supernova must be considered. The optical/UV thermal component observed in 060218 is not seen here: if the extinction is similar we would expect a shock breakout similar to 060218 to be two or more times fainter in 100316D and with the relatively brighter host galaxy it is perhaps no surprise that early optical emission is not detected with UVOT. The presence of a thermal component in the prompt γ -ray emission of BATSE (Burst and Transient Source Experiment) GRBs, in addition to non-thermal emission, was proposed by Ryde (2004). The discovery of thermal components in the *Swift* XRT X-ray spectra shown here for 100316D and in Campana et al. (2006) for 060218 will therefore be important to consider in future studies of GRB prompt emission. The dominant component of the high energy emission in 100316D remains the synchrotron-like non-thermal spectrum common to all types of GRB (with and without SNe) thought to originate in internal shocks in a relativistic jet. The long duration of the early X-ray emission is curious, and exceedingly rare, perhaps suggesting a greater reservoir of material is available to feed the central engine and prolong its activity.

The discovery of GRB 100316D and its associated supernova SN 2010bh and the analyses of its high energy emission and host galaxy properties presented here illustrates the diversity in GRB-SNe characteristics that must be under-

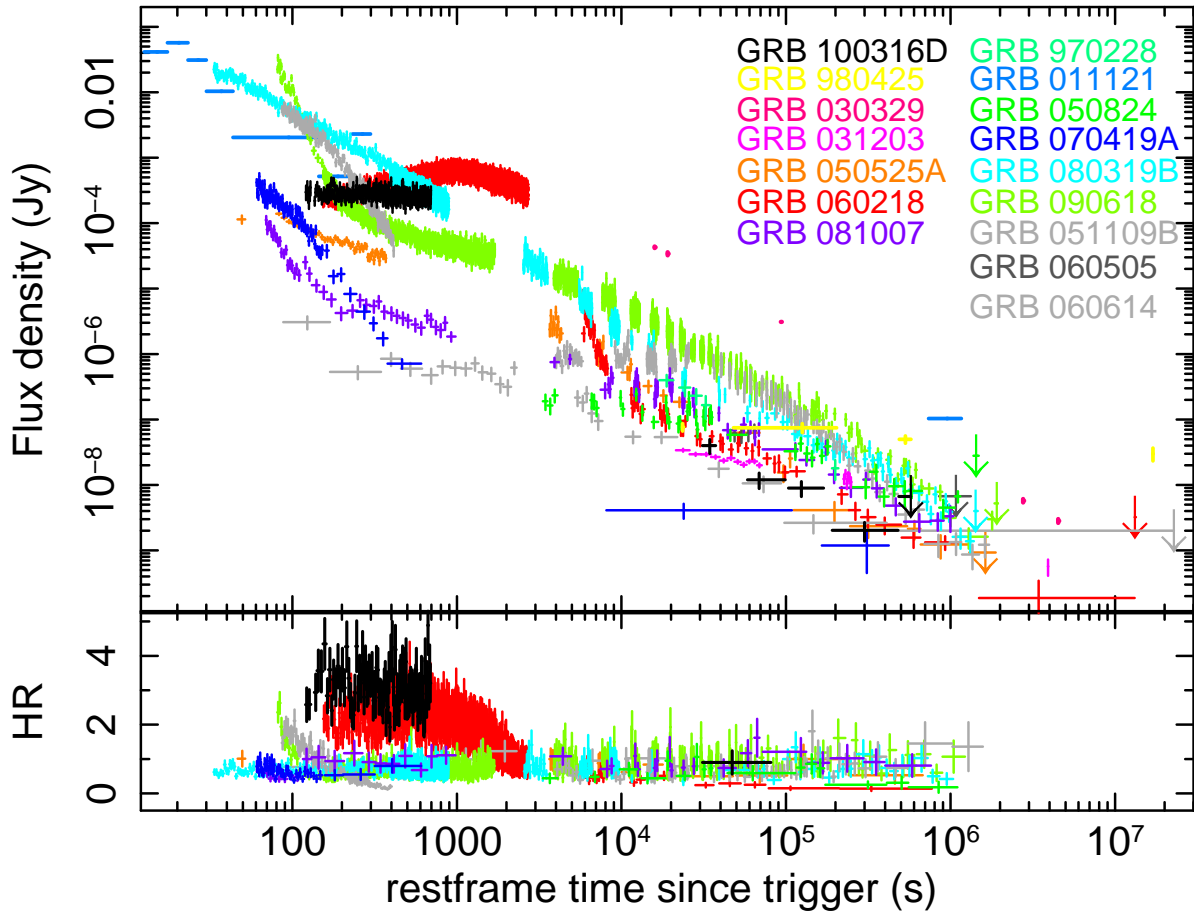


Figure 7. X-ray light curves against time since trigger in flux density at 1.7 keV for a selection of long GRBs with associated supernovae (either spectroscopically confirmed - generally coloured in shades of red with GRB 100316D in black, or photometrically determined - shades of blue and green), two nearby long GRBs with no observed supernovae to deep limits and a further long GRB likely at $z \leq 0.1$ with no reported supernova (grey shades). The lower panel shows the hardness ratios for the *Swift* XRT-observed GRBs, derived from the 1.5–10 keV and 0.3–1.5 keV count rate light curves in the same colour scheme. References for the data sources: 100316D², 980425 (Pian et al. 2000), 030329 (Willingale et al. 2004), 031203 (Watson et al. 2004), 050525A (Blustin et al. 2006, and ²), 060218², 081007², 970228 (Costa et al. 1997; De Pasquale et al. 2006), 011121 (Piro et al. 2005), 050824², 070419A², 080319B², 090618², 051109B², 060505², 060614².

Table 5. Host galaxies of nearby GRB-SNe. The absolute magnitudes M_B were taken from the compilation of Levesque et al. (2010).

GRB	T_e oxygen abundance ($12 + \log(\text{O}/\text{H})$)	Host type	Absolute magnitude M_B	References
980425	8.25 (GRB site)	Dwarf spiral	-17.6	Sollerman et al. (2005); Hammer et al. (2006)
	8.39 (nearby WR region)			
020903	7.97	Irr	-18.8	Hammer et al. (2006)
030329	7.72	Irr	-16.5	Levesque et al. (2010)
031203	8.02 ± 0.15 (integrated)	Irr	-21.0	Prochaska et al. (2004)
060218	$7.54^{+0.16}_{-0.1}$ (integrated)	Irr	-15.9	Wiersema et al. (2007)
100316D	8.23 ± 0.15 (source A)	Spiral? Irr?	-18.8	This work

stood if we are to fully appreciate the relationship between GRBs and core-collapse SNe.

9 ACKNOWLEDGMENTS

This work made use of data supplied by the UK *Swift* Science Data Centre at the University of Leicester. Based on

observations made with ESO Telescopes at the La Silla or Paranal Observatories under programme IDs 084.D-0939, 083.A-0644 and 084.A-0260(B). Based on observations made with the NASA/ESA Hubble Space Telescope, obtained at the Space Telescope Science Institute, which is operated by the Association of Universities for Research in Astronomy, Inc., under NASA contract NAS 5-26555; these observations are associated with programme 11709. We thank STScI

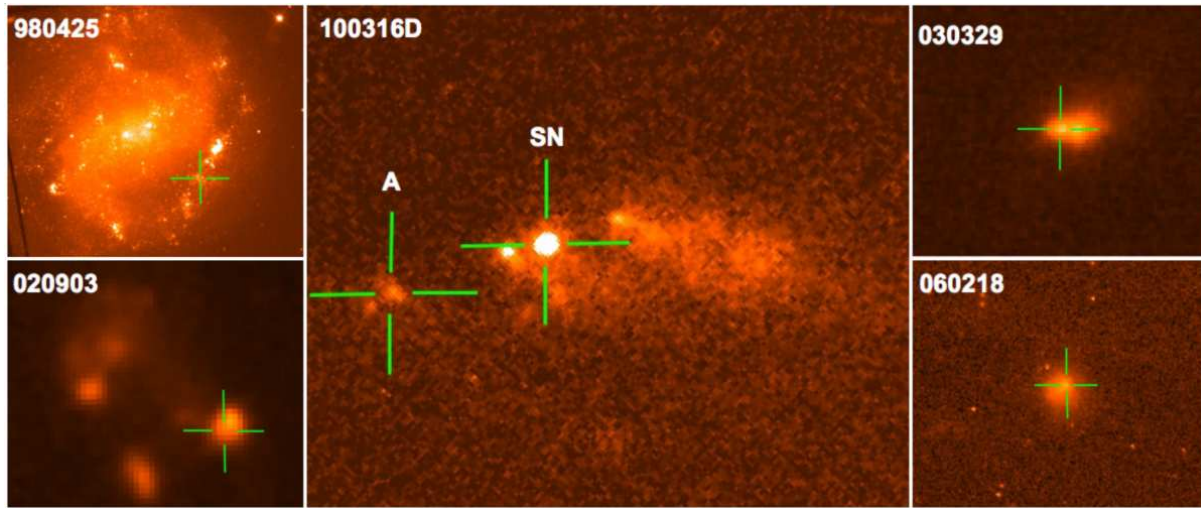


Figure 8. A mosaic of the host galaxies of spectroscopically confirmed supernovae, associated with GRBs, and imaged by the Hubble Space Telescope. The centre image shows the host of GRB 100316D, while other examples are shown in smaller insets. The physical scale across each image is approximately 7 kpc, and the positions of source A and of the SN are marked with crosshairs. Note, in the case of GRB 060218 and GRB 100316D there is still some contamination from the supernova at the time of the image.

staff for their efforts in implementing the HST ToO observation, particularly Alison Vick. We acknowledge the wider *Swift* team for their many contributions. RLCS, KW, AR, JPO, KLP and PAE acknowledge financial support from STFC. Financial support of the British Council and Platform Beta Techniek through the Partnership Programme in Science (PPS WS 005) is gratefully acknowledged (KW). The Dark Cosmology Centre is funded by the Danish National Research Foundation. DNB acknowledges NASA contract NAS5-00136. AJvdH was supported by an appointment to the NASA Postdoctoral Program at the MSFC, administered by Oak Ridge Associated Universities through a contract with NASA.

REFERENCES

- Alard C., 2000, *A&AS*, 144, 363
 Amati L., 2006, *MNRAS*, 372, 233
 Amati L., Della Valle M., Frontera F., Malesani D., Guidorzi C., Montanari E., Pian E., 2007, *A&A*, 463, 913
 Arnaud K., 1996, *ASPC*, 101, 17
 Asplund M.M., Grevesse N., Sauval A.J., Allende-Prieto C., Kiselman D., 2004, *A&A*, 417, 751
 Band D. et al., 1993, *ApJ*, 413, 281
 Barthelmy S. et al., 2005, *Space Sci. Rev.*, 120, 143
 Blustin A.J. et al., 2006, *ApJ*, 637, 901
 Bufano F. et al., 2010, *GCN Circ.* 10543
 Burrows D.N. et al., 2005, *Space Sci. Rev.*, 120, 165
 Cantiello M., Yoon S.-C., Langer N., Livio M., 2007, *A&A*, 465, L29
 Campana S. et al., 2006, *Nature*, 442, 1008
 Campana S., Thoene C.C., de Ugarte Postigo A., Tagliaferri G., Moretti A., Covino S., 2010, *MNRAS*, 402, 2429
 Chapman R., Tanvir N.R., Priddey R.S., Levan A.J., 2007, *MNRAS*, 382, L21
 Chornock R. et al., 2010, *ApJL* submitted, arXiv:1004.2262
 Christensen L., Vreeswijk P.M., Sollerman J., Thöne C.C., L Floc'h E., Wiersema K., 2008, *A&A*, 490, 45
 Cobb B.E., Bailyn C.D., van Dokkum P.G., Natarajan P., 2006, *ApJ*, 645, L113
 Costa E. et al., 1997, *Nature*, 387, 783
 De Pasquale M. et al., 2006, *A&A*, 455, 813
 Della Valle M. et al., 2006, *ApJ*, 642, L103
 D'Odorico S. et al., 2006, *Proceedings of the SPIE*, Volume 6269, p.98
 Evans P.A. et al., 2007, *A&A*, 469, 379
 Evans P.A. et al., 2009, *MNRAS*, 397, 1177
 Fan Y.-Z., Zhang B.-B., Xu D., Liang E.-W., Zhang B., 2010, *ApJ* submitted, arXiv:1004.5267
 Ferrero P. et al., 2006, *A&A*, 457, 857
 Fruchter A.S. et al., 2006, *Nature*, 441, 463
 Fynbo J.P.U. et al., 2006, *Nature*, 444, 1047
 Fynbo J.P.U. et al., 2009, *ApJS*, 185, 526
 Galama T.J. et al., 1998, *Nature*, 395, 670
 Gal-Yam A. et al., 2006, *Nature*, 444, 1053
 Gehrels N. et al., 2004, *ApJ*, 611, 1005
 Gehrels N. et al., 2008, *ApJ*, 689, 1161
 Ghisellini G., Ghirlanda G., Tavecchio F., 2007, *MNRAS*, 382, L77
 Goldoni P. et al., 2006, *SPIE*, 6269, 80
 Gonzalez Delgado R.M., Leitherer C., Heckman T.M., 1999, *ApJS*, 125, 489
 Hammer F., Flores H., Schaerer D., Dessauges-Zavadsky M., Le Floc'h E., Puech M., 2006, *A&A*, 454, 103
 Hjorth J. et al., 2003, *Nature*, 423, 847
 Hurkett C.P. et al., 2008, *ApJ*, 679, 587
 Izotov Y.I., Thuan, T.X., Lipovetsky V.A., 1994, *ApJ*, 435, 647
 Jakobsson P. et al., 2006, *A&A*, 447, 897
 Kalberla P.M.W., Burton W.B., Hartmann D., Arnal E.M., Bajaja E., Morras R., Poppel W.G.L., 2005, *A&A*, 440, 775
 Kaneko Y. et al., 2007, *ApJ*, 654, 385

- Kennicutt R.C., 1998, *ARA&A*, 36, 189
- Kulkarni S.R. et al., 1998, *Nature*, 395, 663
- Levan A.J., Tanvir N.R., D’Avanzo P., Vergani S.D., Malesani D., 2010, *GCN Circ.* 10523
- Levesque E.M., Berger E., Kewley L.J., Bagley M.M., 2010, *AJ*, 139, 694
- Liang E., Zhang B., Virgili F., Dai Z.G., 2007, *ApJ*, 662, 1111
- Malesani D. et al., 2004, *ApJ*, 609, L5
- Mazzali P.A. et al., 2005, *Science*, 308, 1284
- Mazzali P.A. et al., 2006, *Nature*, 442, 1018
- Mirabal N., Halpern J.P., An D., Thorstensen J.R., Terndrup D.M., 2006, *ApJ*, 643, L99
- Modjaz M. et al., 2006, *ApJ*, 645, L21
- Oates S.R., De Pasquale M., Stamatikos M., 2010, *GCN Circ.* 10520
- Osterbrock, 1989, *Astrophysics of gaseous nebulae and active galactic nuclei*, University Science Books
- Paragi Z. et al., 2010, *Nature*, 463, 516
- Pei Y.C., 1992, *ApJ*, 395, 130
- Perley D.A., Foley R.J., Bloom J.S., Butler N.R., 2006, *GCN Circ.* 5387
- Pian E., Antonelli L.A., Piro L., Feroci M., 1998, *GCN Circ.* 158
- Pian E. et al., 2000, *ApJ*, 536, 778
- Pian E. et al., 2006, *Nature*, 442, 1011
- Piro L. et al., 2005, *ApJ*, 623, 314
- Poole T.S. et al., 2008, *MNRAS*, 383, 627
- Prochaska J.X. et al., 2004, *ApJ*, 611, 200
- Rees M.J., Mészáros P., 1994, *ApJ*, 430, L93
- Roming P.W.A. et al., 2005, *Space Sci. Rev.*, 120, 95
- Ryde F., 2004, *ApJ*, 614, 827
- Sakamoto T. et al., 2008, *ApJS*, 175, 179
- Sari R., Piran T., Narayan R., 1998, *ApJ*, 497, L17
- Schlegel D.J., Finkbeiner D.P., Davis M., 1998, *ApJ*, 500, 525
- Soderberg A.M. et al., 2006, *Nature*, 442, 1014
- Soderberg A.M. et al., 2010, *Nature*, 463, 513
- Sollerman J., Östlin, G., Fynbo J.P.U., Hjorth J., Fruchter A., Pedersen K., 2005, *NewA*, 11, 103
- Sollerman J. et al., 2006, *A&A*, 454, 503
- Stanek K.Z. et al., 2003, *ApJ*, 591, L17
- Stamatikos M. et al., 2010, *GCN Circ.* 10496
- Starling R.L.C. et al., 2008, *MNRAS*, 384, 504
- Starling R.L.C., Evans P.A., Stamatikos M., 2010, *GCN Circ.* 10519
- Stratta G., Perri M., Siegel M.H., Krimm H.A., Barthelmy S.D., Roming P., Burrows D.N., Gehrels N., 2009, *GCN Report* 212.1
- Svensson K.M., Levan A.J., Tanvir N.R., Fruchter A.S., Strolger L.G., 2010, *MNRAS* in press
- Tanvir N.R. et al., 2010, *ApJ* in press, arXiv:0812.1217
- Toma K., Ioka K., Sakamoto T., Nakamura T., 2007, *ApJ*, 659, 1420
- Vergani S., Levan A.J., D’Avanzo P., Covino S., Malesani D., Hjorth J., Tanvir N.R., Antonelli L.A., 2010, *GCN Circ.* 10513
- Verner D.A., Ferland G.J., Korista K.T., Yakovlev D.G., 1996, *ApJ*, 465, 487
- Watson D. et al., 2004, *ApJ*, 605, L101
- Watson D., Hjorth J., Fynbo J.P.U., Jakobsson P., Foley S., Sollerman J., Wijers R.A.M.J., 2007, *ApJ*, 660, L101
- Waxman E., Mészáros P., Campana S., 2007, *ApJ*, 667, 351
- Wiersema K. et al., 2007, *A&A*, 464, 529
- Wiersema K., D’Avanzo P., Levan A.J., Tanvir N.R., Malesani D., Covino S., 2010, *GCN Circ.* 10525
- Willingale R. et al., 2004, *MNRAS*, 349, 41
- Wilms J., Allen A., McCray R., 2000, *ApJ*, 542, 914
- Woosley S.E., Bloom J.S., 2006, *ARA&A*, 44, 507
- Zeh A., Klose S., Hartmann D.H., 2005, in *Proc. 22nd Texas Symp. on Relativistic Astrophysics*, ed. P. Chen et al. (Stanford: SLAC), arXiv:astro-ph/0503311

This paper has been typeset from a \TeX / \LaTeX file prepared by the author.